Circular Dichroism and Magnetic Circular Dichroism Spectroscopy of the Catalytically Competent Ferrous Active Site of Phenylalanine Hydroxylase and Its Interaction with Pterin Cofactor

Jyllian N. Kemsley,[†] Nataša Mitić,[‡] Kelly Loeb Zaleski,[†] John P. Caradonna,*[,§] and Edward I. Solomon*[,†]

Contribution from the Departments of Chemistry, Stanford University, Stanford, California 94305-5080, Yale University, New Haven, Connecticut 06520, Boston University, Boston, Massachusetts 02215

Received September 16, 1998

Abstract: The tetrahydrobiopterin-dependent enzyme phenylalanine hydroxylase (PAH) contains one non-heme iron atom per subunit that is required for reactivity. We have applied circular dichroism (CD), magnetic circular dichroism (MCD), and variable-temperature, variable-field (VTVH) MCD spectroscopies to investigate the geometric and electronic structure of the catalytically relevant ferrous active site and its interaction with the cofactor analogue 5-deaza-6-methyltetrahydropterin, in the absence and presence of substrate. Excited-state ligand field CD and MCD data indicate that the six-coordinate ferrous active site of the resting and *N*-ethylmaleimide-activated enzyme is not perturbed by the addition of pterin cofactor in the absence of substrate ($\Delta^5E_g = 1900$ cm^{-1}, $10Dq = 9850$ cm^{-1}). VTVH MCD analysis yields a ground-state splitting also consistent with an unperturbed six-coordinate ferrous site ($\Delta^5T_{2g} = -285$ or -1150 cm^{-1}). Addition of pterin in the presence of L-phenylalanine (L-Phe), however, results in large splittings of the excited- and ground-state orbitals ($\Delta^5E_g > 4600$ cm^{-1}, $10Dq < 8800$ cm^{-1}; $\Delta^5T_{2g} = +985$ cm^{-1}) that are indicative of a square-pyramidal five-coordinate ferrous site. Our results provide molecular-level insight into the observed sequential mechanistic order for PAH, L-Phe + BH_4 + O_2, and offer the first evidence of an open coordination position on the iron prior to binding and activation of dioxygen. This directly implicates the iron in the coupled hydroxylation of substrate and cofactor, and shows that a highly reactive oxygen intermediate can be generated only when both are present.

Introduction

A wide range of essential biological functions involving the binding and activation of dioxygen are catalyzed by enzymes containing mononuclear non-heme iron active sites.[1,2] These enzymes may be classified according to the reactions they catalyze: dismutation (e.g., superoxide dismutase[3]), oxidation (e.g., isopenicillin *N*-synthase[4]), hydroperoxidation (e.g., lipoxygenases[5]), and dioxygenation. The dioxygenases can be divided further into extra- and intradiol dioxygenases (e.g., catechol 2,3-dioxygenase and protocatechuate 3,4-dioxygenase, respectively[6,7]), *cis*-dihydroxylases (e.g., phthalate dioxygenase[8]), α-ketoglutarate-dependent hydroxylases (e.g., clavaminate synthase[9]), and pterin-dependent hydroxylases.[10]

The tetrahydrobiopterin (BH_4)-dependent hydroxylases are involved in activation of O_2 for specific oxygenation reactions, regulation of aromatic amino acid metabolism, and mediation for proper brain function.[10] Phenylalanine, tyrosine, and tryptophan hydroxylases perform critical and potentially rate-limiting steps in phenylalanine catabolism (PAH),[11,12] epinephrine/catecholamine biosynthesis (TyrH),[13−15] and serotonin biosynthesis (TrpH),[16] respectively. It has been well-established for PAH that clinically significant conditions may arise from altered pterin-dependent hydroxylase activity and such effects are suspected for TyrH and TrpH. Liver PAH functions in homeostatic regulation of plasma levels of L-phenylalanine (L-Phe); dysfunction of PAH may lead to an accumulation of neurotoxic L-Phe metabolites and to the genetic disorder phenylketonuria (PKU).[17] This condition affects one in 10 000 infants in the

[†] Department of Chemistry, Stanford University.
[‡] Department of Chemistry, Yale University.
[§] Department of Chemistry, Boston University.

(1) Feig, A. L.; Lippard, S. J. *Chem. Rev.* **1994**, *94*, 759−805.
(2) Que, L., Jr.; Ho, R. Y. N. *Chem. Rev.* **1996**, *96*, 2607−2624.
(3) Stoddard, B. L.; Howell, P. L.; Ringe, D.; Petsko, G. A. *Biochemistry* **1990**, *29*, 8885−8893.
(4) Baldwin, J. E.; Bradley, M. *Chem. Rev.* **1990**, *90*, 1079−1088.
(5) Samuelsson, B.; Dahlén, S.-E.; Lindgren, J. å.; Rouzer, C. A.; Serhan, C. N. *Science* **1987**, *237*, 1171−1176.
(6) Que, L., Jr. In *Iron Carriers and Iron Proteins*; Loehr, T. M., Ed.; Physical Bioinorganic Chemistry Series, Vol. 5; VCH: New York, 1989; pp 467−524.
(7) Lipscomb, J. D.; Orville, A. M. In *Degradation of Environmental Pollutants by Microorganisms and Their Metalloenzymes*; Sigel, H., Sigel, A., Eds.; Metal Ions in Biological Systems, Vol. 28; Marcel Dekker: New York, 1992; pp 243−298.
(8) Batie, C. J.; LaHaie, E.; Ballou, D. P. *J. Biol. Chem.* **1987**, *262*, 1510−1518.
(9) Salowe, S. P.; Marsh, E. N.; Townsend, C. A. *Biochemistry* **1990**, *29*, 6499−6508.
(10) Kappock, T. J.; Caradonna, J. P. *Chem. Rev.* **1996**, *96*, 2659−2756.
(11) Shiman, R. In *Chemistry and Biochemistry of Pterins*; Blakley, R. L., Benkovic, S. J., Eds.; Folates and Pterins, Vol. 2; John Wiley & Sons: New York, 1985; pp 179−249.
(12) Kaufman, S. *Adv. Enzymol. Relat. Areas Mol. Biol.* **1993**, *67*, 77−264.
(13) Fitzpatrick, P. F. *Biochemistry* **1991**, *30*, 6386-6391.
(14) Goodwill, K. E.; Sabatier, C.; Marks, C.; Raag, R.; Fitzpatrick, P. F.; Stevens, R. C. *Nat. Struct. Biol.* **1997**, *4*, 578−585.
(15) Kaufman, S.; Kaufman, E. E. In *Chemistry and Biochemistry of Pterins*; Blakley, R. L., Benkovic, S. J., Eds.; Folates and Pterins, Vol. 2; John Wiley & Sons: New York, 1985; pp 251−352.
(16) Kuhn, D. M.; Ruskin, B.; Lovenberg, W. *J. Biol. Chem.* **1980**, *255*, 4137−4143.

10.1021/ja9833063 CCC: $18.00
Published on Web 01/29/1999

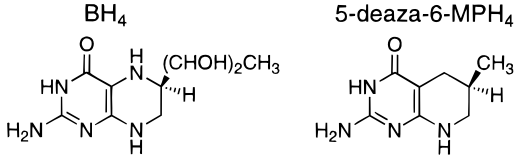

Figure 1. Structures of tetrahydrobiopterin (BH_4) and its analogue 5-deaza-6-methyltetrahydropterin (5-deaza-6-MPH_4).

United States and its principal clinical manifestation is severe, progressive mental retardation.

It is believed that the three pterin-dependent hydroxylases contain similar active sites due to the high degree of sequence homology in the catalytic domains and the similarity of cofactor and substrate requirements.[11,15,18] Rat hepatic PAH (phenylalanine 4-monooxygenase, EC 1.14.16.1) is the most extensively studied of the enzymes due to its abundance, solubility, and relative ease of purification.[10−12] PAH exists as a homodimer or tetramer of 51.7 kDa subunits,[19,20] each of which contains a non-heme iron that is required for reactivity.[21,22] During the hydroxylation of phenylalanine, the enzyme uses dioxygen and BH_4 (Figure 1) to generate tyrosine and 4a-hydroxytetrahydropterin[23] in a coupled reaction where dioxygen is partitioned between the phenolic hydroxy group of tyrosine and the 4a-carbinolamine form of the oxidized pterin. A 4a-hydroperoxytetrahydropterin intermediate has been proposed[24] but not observed for the hydroxylation reaction. The oxidized pterin is cycled back to BH_4 via 4a-carbinolamine dehydratase (DCoH) and dihydropteridine reductase (DHPR).[10]

Both L-Phe and BH_4 have regulatory interactions with PAH in addition to their roles in the catalytic cycle. BH_4 reduces PAH from the ferric to the ferrous state,[25−28] and L-Phe activates the enzyme through cooperative binding to an allosteric effector site (distinct from the catalytic site) where it remains bound through multiple catalytic cycles.[11,20,29,30] The consequent formation of reduced, activated PAH is concurrent with the appearance of a catalytically competent species.[11] The L-Phe-induced transition between the resting low-affinity ("tense") state (PAH^T) and the activated high-affinity ("relaxed") state (PAH^R) has a large energetic barrier of ∼34 kcal mol^{-1} and is accompanied by a significant structural rearrangement of the protein.[20,31] Additionally, the quaternary structure of PAH exists in equilibrium between the dimeric and tetrameric form, and activation by L-Phe serves to shift this equilibrium to favor the tetramer.[32] The apparent elimination of the requirement for L-Phe activation can be accomplished by using detergents (lysolecithin), proteases (α-chymotrypsin), or sulfhydryl-modifying reagents (*N*-ethylmaleimide), which also induce dimer formation.[33−35] Because BH_4 will inhibit L-Phe-induced conversion of PAH^T to PAH^R,[11,20,29,36−38] an ordered sequential mechanism is observed for the resting enzyme with its natural substrates: L-Phe + BH_4 + O_2.[31,38,39] This inhibition of activation is specific for BH_4; for example, 6-methyltetrahydropterin (6-MPH_4), a cofactor analogue, is 1000-fold less effective than BH_4.[38] It has been proposed that the dihydroxypropyl side chain of BH_4 (Figure 1) may block the substrate binding site thereby restricting access of L-Phe.[37]

Most studies previously reported on the iron active site of PAH have been concerned with the ferric form of the enzyme, which is more spectroscopically accessible.[27,40] The crystal structure of the enzyme has also been reported on the ferric form.[41,42] The active form of the enzyme, however, is the reduced ferrous state and thus it is critically important to define the nature of the ferrous site and its involvement in the catalytic mechanism of PAH. We have employed a protocol utilizing circular dichroism (CD), magnetic circular dichroism (MCD), and variable-temperature, variable-field (VTVH) MCD spectroscopies to probe the geometric and electronic structure of high-spin $S = 2$ Fe^{2+} centers.[43−46] The ^5D ground state for the d^6 Fe^{2+} free ion is split under octahedral symmetry into a $^5T_{2g}$ ground state (with the extra electron in the d_{yz}, d_{xz}, or d_{xy} orbital) and a ^5E_g excited state (extra electron in the $d_{x^2-y^2}$ or d_{z^2} orbital), separated by $10Dq$ (∼10 000 cm^{-1} for biologically relevant nitrogen and oxygen ligands). The splitting of the ^5E_g excited state ($\Delta^5E_g \equiv d_{x^2-y^2} - d_{z^2}$) is sensitive to the coordination number and geometry of the site, and near-IR CD and MCD spectroscopy allow for direct observation of these d → d transitions. In general, six-coordinate distorted octahedral ferrous sites show two transitions centered at ∼10 000 cm^{-1} and split by $|\Delta^5E_g| < 2000$ cm^{-1}; five-coordinate sites show two transitions at ∼10 000 and ∼5000 cm^{-1} ($|\Delta^5E_g| \approx 5000$ cm^{-1}) which are shifted to lower energy on going from a square pyramidal to a trigonal bipyramidal site; and distorted four-coordinate sites show two transitions in the region of 4000−7000 cm^{-1} [i.e., $10Dq(T_d) = (-4/9)10Dq(O_h)$].

VTVH MCD can be used to obtain further insight into ground-state electronic structure. The temperature and field dependence of the MCD intensity for non-Kramers ferrous centers is characterized by nesting behavior (i.e., nonsuperim-

(17) Scriver, C. R.; Eisensmith, R. C.; Woo, S. L. C.; Kaufman, S. *Annu. Rev. Genet.* **1994**, *28*, 141−165.
(18) Kuhn, D. M.; Lovenberg, W. In *Chemistry and Biochemistry of Pterins*; Blakley, R. L., Benkovic, S. J., Eds.; Folates and Pterins, Vol. 2; John Wiley & Sons: New York, 1985; pp 353−382.
(19) Kaufman, S. *Adv. Enzymol.* **1971**, *35*, 245−319.
(20) Shiman, R.; Gray, D. W. *J. Biol. Chem.* **1980**, *255*, 4793−4800.
(21) Fisher, D. B.; Kirkwood, R.; Kaufman, S. *J. Biol. Chem.* **1972**, *247*, 5161−5167.
(22) Gottschall, D. W.; Dietrich, R. F.; Benkovic, S. J.; Shiman, R. *J. Biol. Chem.* **1982**, *257*, 845−849.
(23) Dix, T. A.; Bollag, G. E.; Domanico, P. L.; Benkovic, S. J. *Biochemistry* **1985**, *24*, 2955−2958.
(24) Dix, T. A.; Benkovic, S. J. *Acc. Chem. Res.* **1988**, *21*, 101−107.
(25) Shiman, R. *J. Biol. Chem.* **1980**, *255*, 10029−10032.
(26) Marota, J. J. A.; Shiman, R. *Biochemistry* **1984**, *23*, 1303−1311.
(27) Wallick, D. E.; Bloom, L. M.; Gaffney, B. J.; Benkovic, S. J. *Biochemistry* **1984**, *23*, 1295−1302.
(28) Hill, M. A.; Marota, J. J. A.; Shiman, R. *J. Biol. Chem.* **1988**, *263*, 5646−5655.
(29) Shiman, R.; Gray, D. W.; Pater, A. *J. Biol. Chem.* **1979**, *254*, 11300−11306.
(30) Shiman, R.; Jones, S. H.; Gray, D. W. *J. Biol. Chem.* **1990**, *265*, 11633−11642.
(31) Kappock, T. J.; Harkins, P. C.; Friedenberg, S.; Caradonna, J. P. *J. Biol. Chem.* **1995**, *270*, 30532−30544.
(32) Kappock, T. J. Ph.D. Thesis, Yale University, New Haven, CT, 1996.
(33) Fisher, D. B.; Kaufman, S. *J. Biol. Chem.* **1973**, *248*, 4345−4353.
(34) Parniak, M. A.; Kaufman, S. *J. Biol. Chem.* **1981**, *256*, 6876−6882.
(35) Phillips, R. S.; Parniak, M. A.; Kaufman, S. *Biochemistry* **1984**, *23*, 3836−3842.
(36) Døskeland, A. P.; Døskeland, S. O.; Øgreid, D.; Flatmark, T. *J. Biol. Chem.* **1984**, *259*, 11242−11248.
(37) Shiman, R.; Xia, T.; Hill, M. A.; Gray, D. W. *J. Biol. Chem.* **1994**, *269*, 24647−24656.
(38) Xia, T.; Gray, D. W.; Shiman, R. *J. Biol. Chem.* **1994**, *269*, 24657−24665.
(39) Tourian, A. *Biochim. Biophys. Acta* **1971**, *242*, 345−354.
(40) Bloom, L. M.; Benkovic, S. J.; Gaffney, B. J. *Biochemistry* **1986**, *25*, 4204−4210.
(41) Erlandsen, H.; Fusetti, F.; Martínez, A.; Hough, E.; Flatmark, T.; Stevens, R. C. *Nat. Struct. Biol.* **1997**, *4*, 995−1000.
(42) Fusetti, F.; Erlandsen, H.; Flatmark, T.; Stevens, R. C. *J. Biol. Chem.* **1998**, *273*, 16962−16967.
(43) Whittaker, J. W.; Solomon, E. I. *J. Am. Chem. Soc.* **1988**, *110*, 5329−5339.
(44) Solomon, E. I.; Zhang, Y. *Acc. Chem. Res.* **1992**, *25*, 343−352.
(45) Solomon, E. I.; Pavel, E. G.; Loeb, K. E.; Campochiaro, C. *Coord. Chem. Rev.* **1995**, *144*, 369−460.
(46) Pavel, E. G.; Kitajima, N.; Solomon, E. I. *J. Am. Chem. Soc.* **1998**, *120*, 3949−3962.

posing isotherms when MCD intensity data are plotted vs $\beta H/2kT$). For negative zero-field splitting (ZFS) systems ($D < 0$; $M_S = \pm 2$ lowest in energy), this behavior is due to the rhombic zero-field splitting (δ) of the $M_S = \pm 2$ doublet ground state, which shows a nonlinear magnetic field dependence.[43] The value of δ is sensitive to the site geometry and generally is found to be larger (i.e., more nested) for distorted six-coordinate ferrous sites ($3 < \delta < 7$ cm^{-1}) than for five-coordinate sites ($\delta < 4$ cm^{-1}).[45,46] Ground-state parameters are obtained by computationally fitting the experimental VTVH MCD data to an orientation-averaged intensity expression that includes the rhombic and Zeeman splitting of a non-Kramers doublet (δ and $g_{||}$), as well as the transition polarization ratio (M_z/M_{xy}) and contributions from linear temperature-independent B-terms and low-lying excited states (see refs 45 and 46 for details). This analysis has also been extended to include positive ZFS systems ($D > 0$; $M_S = 0$ lowest),[46,47] which can show qualitatively similar saturation magnetization behavior arising from off-axis Zeeman mixing of a pseudo-doublet ground state comprised of the $M_S = 0$ and one component of the $M_S = \pm 1$ sublevels. Such systems can be distinguished from negative ZFS by a large nesting behavior and therefore splitting of the ground state (by $\sim D$ instead of δ) and the presence of an additional MCD-inactive low-lying singlet excited state (the other component of $M_S = \pm 1$).

The ground-state parameters obtained from the saturation magnetization analysis are directly related to the splitting of the $^5T_{2g}$ ground state ($\Delta \equiv d_{xz,yz} - d_{xy}$ and $V \equiv d_{xz} - d_{yz}$) so that the t_{2g} orbital energies can be determined.[45] Larger values of δ are associated with smaller values of Δ as expected for six-coordinate sites, and smaller δ values are associated with larger Δ values as for five-coordinate systems where the open coordination position causes a larger splitting of the d_{xy} and $d_{xz,yz}$ orbitals. Ligand field MCD and VTVH MCD in combination therefore provide a complete description of the d-orbitals for a given ferrous site, which provides information on the geometric and electronic structure of the active site. This methodology has now been applied to a variety of mononuclear non-heme ferrous enzymes to probe oxygen and substrate reactivity and to gain molecular-level insight into the catalytic mechanism.[43,48−52]

Previously, we have reported results using these techniques combined with X-ray absorption spectroscopy (XAS) to probe for the first time the effects of substrate activation on the catalytically relevant ferrous active site of PAH[53] (all further references to PAH will be of the ferrous enzyme unless otherwise indicated). From the ~2000 cm^{-1} splitting and relatively low energies of the two d → d transitions observed in the near-IR MCD spectrum, it was found that the iron site of resting PAH^T[ ] (empty brackets indicate the absence of either substrate or cofactor in the active site cavity) is six-coordinate distorted octahedral with a first coordination sphere comprised of significant oxygen ligation. Activation of the enzyme to PAH^R[ ] via allosteric or nonallosteric (using *N*-ethylmaleimide, NEM) methods does not perturb the geometric structure of the ferrous active site based on the comparable d-orbital transition energies. The crystal structure of a dimeric form of the catalytic domain of Fe^{3+}PAH, indicating two histidines, a monodentate glutamate, and three water ligands, has confirmed this description for the ferric active site.[41] The addition of substrate to either the resting or activated enzyme, however, results in a geometric perturbation to the metal center characterized by a shift to higher energy of the d → d transitions reflecting an increase in ligand field strength.[53] This is attributed to a rearrangement of the existing active site ligands, including an increase in the relative number of ligands contributing to the inner vs the outer subshell of the first coordination sphere. Such a structural rearrangement may be implicated in the orientation of the substrate for completely coupled hydroxylation.

Scheme 1

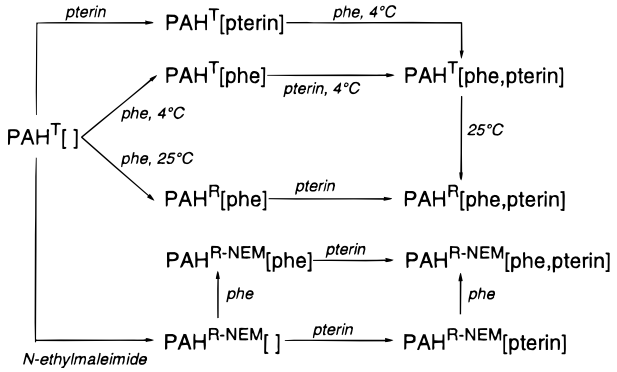

To understand the involvement of the pterin cofactor and the complex mechanistic behavior of PAH, we have now extended our use of ligand field and VTVH MCD spectroscopy to investigate the interactions of the ferrous active site of PAH with a nonredox-active pterin analogue that is a competitive inhibitor of BH_4, 5-deaza-6-methyltetrahydropterin (5-deaza-6-MPH_4, Figure 1).[37] This approach simplifies the preparative aspects involved in using pterins capable of undergoing redox reactions but effectively probes for possible active site structural changes associated with inhibition and regulation of the enzyme. A summary of the relevant protein forms is given in Scheme 1. These results offer the first direct information about the interplay of Fe^{2+}, L-Phe, and pterin cofactor in PAH reactivity and provide insight into the catalytic mechanism.

Experimental Section

Chemicals. All commercial reagents were of the highest grade available and were used without further purification. L-Phe, 4-morpholinepropanesulfonic acid (MOPS), and other supplies were from Sigma (St. Louis, MO). Sodium dithionite and D_2O (99.9 atom % D) were from Aldrich (Milwaukee, WI), and KCl was from Mallinckrodt (Paris, KY). Glycerol-d_3 (98 atom % D) was from Cambridge Isotopes Laboratories (Andover, MA).

PAH Isolation. Recombinant rat liver PAH was overexpressed in *Escherichia coli* with use of a modification of the protocol previously described.[31] BL21(DE3) cells, freshly transformed by the method of Hanahan,[54] were used as the source of protein-producing cultures. These were grown to an $Abs_{550} = 1.8$ in 10 L of modified 2xYT media (containing 160 g of Bacto-tryptone, 100 g of yeast, 85 mM NaCl, 40 mL of glycerol, 25 μM $FeCl_3$, 0.5 g of ampicillin, 2 mM $MgSO_4$, 100 μM $CaCl_2$, 12 μM H_3BO_3, 8 μM $(NH_4)_6Mo_7O_{24}\cdot 4H_2O$, and 6 μM KI)

(47) Campochiaro, C.; Pavel, E. G.; Solomon, E. I. *Inorg. Chem.* **1995**, *34*, 4669−4675.
(48) Mabrouk, P. A.; Orville, A. M.; Lipscomb, J. D.; Solomon, E. I. *J. Am. Chem. Soc.* **1991**, *113*, 4053−4061.
(49) Pavel, E. G.; Martins, L. J.; Ellis, W. R., Jr.; Solomon, E. I. *Chem. Biol.* **1994**, *1*, 173−183.
(50) Pavlosky, M. A.; Zhang, Y.; Westre, T. E.; Gan, Q.-F.; Pavel, E. G.; Campochiaro, C.; Hedman, B.; Hodgson, K. O.; Solomon, E. I. *J. Am. Chem. Soc.* **1995**, *117*, 4316−4327.
(51) Loeb, K. E.; Zaleski, J. M.; Westre, T. E.; Guajardo, R. J.; Mascharak, P. K.; Hedman, B.; Hodgson, K. O.; Solomon, E. I. *J. Am. Chem. Soc.* **1995**, *117*, 4545−4561.
(52) Pavel, E. G.; Zhou, J.; Busby, R. W.; Gunsior, M.; Townsend, C. A.; Solomon, E. I. *J. Am. Chem. Soc.* **1998**, *120*, 743−753.
(53) Loeb, K. E.; Westre, T. E.; Kappock, T. J.; Mitic, N.; Glasfeld, E.; Caradonna, J. P.; Hedman, B.; Hodgson, K. O.; Solomon, E. I. *J. Am. Chem. Soc.* **1997**, *119*, 1901−1915.
(54) Hanahan, D. *J. Mol. Biol.* **1983**, *166*, 557−580.

and induced with 1 g of isopropyl-1-thio-β-D-galactopyranoside (IPTG) for 6 h at 30 °C in a New Bruswick Instruments fermentor before harvesting. The pH was maintained at 7.6 during the course of the growth, as was vigorous aeration. Antifoam A concentrate was added as necessary. Cells were pelleted at 8000 rpm for 10 min at 4 °C, resuspended in an equal volume of lysis buffer (30 mM Tris, 200 mM KCl, 80 mM L-Phe, pH 7.3 at 4 °C), frozen in liquid nitrogen, and stored at −80 °C until protein purification. These modifications resulted in an increased yield of protein (approximately 2-fold) with no alteration in either the level of protein purity or levels of catalytically competent iron sites (≥98%). Purification of PAH is as described previously,[31] and purified PAH was stored at −80 °C until use. The specific activities of the PAH samples used for spectroscopic analysis were all ≥7.0 units mg^{-1}, where 1 unit = 1 μmol of L-tyrosine min^{-1}. Typically, 30−40 mg of protein were used in the preparation of each sample. Concentration of Fe was determined by atomic absorption spectroscopy as previously described.[31]

Synthesis of 5-deaza-6-methyltetrahydropterin. The cofactor analogue 5-deaza-6-MPH_4 was synthesized from 2,4-diamino-6-hydroxypyrimidine and 3-amino-2-methylacrolein following literature procedures.[55,56] The pterin was reduced over platinum dioxide.[57] Spectroscopic characterization (^{1}H and ^{13}C NMR, and UV−visible absorption) of the oxidized and reduced pterins was equivalent to that reported in the literature.[55−57]

Preparation of PAH^T[5-deaza-6-MPH_4]. All protein manipulations were performed at 4 °C unless otherwise noted. The $Fe^{3+}PAH^T$[ ] samples were diluted to approximately 1 mg mL^{-1} (19.3 μM) in L-Phe-free buffer (100 mM MOPS, 300 mM KCl, pH 7.3). The dilute protein solution was filtered through a 0.45 μm syringe filter to remove particulates and then concentrated in a 50 mL Amicon ultrafiltration device over a YM-30 membrane to a final volume of ∼1 mL. The stock solution of 20 mM 5-deaza-6-MPH_4 was prepared in 0.05 N HCl and an appropriate amount of this stock solution was diluted with 500 mM MOPS buffer to maintain a pH of 7.3. This was then added to the protein sample to give a final ratio of 10 equiv of the cofactor relative to the iron content. The cofactor analogue was allowed to bind for ∼10 min (K_d = 7.4 μM[37]) and the sample was concentrated to a final volume of ∼1 mL. This concentrated sample was placed in a microcentrifuge tube and centrifuged at 14 000 rpm for 3 min to remove any precipated protein. The protein sample was then exchanged five times into 100 mM MOPS, 300 mM KCl, and 10 mM 5-deaza-6-MPH_4 buffer prepared in D_2O and adjusted to pD 7.3 with NaOD. In each exchange, the protein solution was concentrated to ≤1 mL and 5 mL of deuterated buffer were added. Between D_2O exchanges, the PAH solution was centrifuged to remove aggregates and prevent further precipitation. The sample was transferred for the last D_2O exchange into an Amicon 8MC micro-ultrafiltration system with a YM-30 membrane preequilibrated in the D_2O exchange buffer. In the final exchange the protein sample was reduced to ∼200 μL so that the final active Fe concentration was 1.2−2.1 mM. The final aqueous protein concentration was determined by the Bradford dye binding assay as previously described.[31]

To facilitate glass formation for low-temperature MCD experiments, the concentrated aqueous protein solution was diluted with several volumes of 55−65% glycerol-d_3 in deuterated buffer. To ensure complete mixing, the glycerol-d_3 was added slowly with careful manual mixing until a brief centrifugation did not induce phase separation of the two components. The resulting ≥50% glycerol-d_3/PAH solution was concentrated to a final volume of 150−200 μL in an Amicon 8MC micro-ultrafiltration device with a YM-30 membrane. This process was very slow due to the high viscosity of the solution. Periodically during ultrafiltration, the N_2 pressure was slowly released and a small aliquot was drawn to determine the protein concentration by the Bradford assay. Once the desired concentration was obtained, strict anaerobic procedures were used for the remainder of the sample preparation.

The protein sample, with or without glycerol-d_3, was reduced in an Ar box by using a solution of sodium dithionite in D_2O, freshly standardized vs $K_3Fe(CN)_6$ (ferricyanide → ferrocyanide $\Delta\epsilon_{420\ nm}$ = 1020 M^{-1} cm^{-1}). Sufficient dithionite to reduce protein-bound Fe^{3+} was added, causing an immediate bleaching of the characteristic yellow color of Fe^{3+}PAH. The reduced sample was stored at −80 °C until further use. For CD, the sample was thawed under a N_2 atmosphere and injected into a 1 cm path length near-IR cuvette, which was sealed with a Kontes stopcock to prevent air oxidation during the time course of the experiment. The similarly thawed MCD sample was injected into an MCD cell assembled under N_2 with a neoprene spacer (0.3 cm path length) sandwiched between two Infrasil quartz disks and stabilized between two fitted copper plates. The MCD sample was then quick-frozen and stored in liquid N_2 until it was inserted into the crysotat under a flow of He gas. One sample without and one sample with glycerol-d_3 were analyzed by CD, while three samples were subjected to VTVH MCD analysis.

Preparation of PAH^{R-NEM}[5-deaza-6-MPH_4]. One PAH^{R-NEM}[5-deaza-6-MPH_4] sample was prepared by incubating 30 mg of $Fe^{3+}PAH^T$[ ] in 30 mL of buffer (19.3 μM PAH) with 30 μM *N*-ethylmaleimide for 45 min at 25 °C prior to filtration and the first concentration step. These conditions were sufficient to irreversibly activate the enzyme by alkylation of Cys236.[34] The dimeric nature of PAH^{R-NEM} (apparent $M_r(PAH^{R-NEM})$ = 120 kDa, $M_r(PAH^T)$ = 248 kDa) was verified by gel filtration studies by using a Superdex 200 26/60 column (Pharmacia) and elution with 120 mM phosphate buffer, 100 mM NaCl, pH 6.8. All subsequent manipulations were performed as described for the PAH^T[5-deaza-6-MPH_4] sample.

Preparation of PAH^R[L-Phe, 5-deaza-6-MPH_4]. The PAH^R[L-Phe, 5-deaza-6-MPH_4] samples were prepared almost identically to PAH^T[5-deaza-6-MPH_4] except that the 1 mg mL^{-1} (19.3 μM) protein solution was brought to 1.0 mM in L-Phe (>50-fold excess) by using a 100 mM stock solution. The protein solution was then incubated for 10 min at 25 °C, and subsequently filtered prior to the first concentration step. These conditions were sufficient to induce the allosteric conversion required for the generation of a catalytically competent form of the enzyme.[29] Before the D_2O buffer exchange, additional L-Phe was added to bring the final concentration to 10 mM. The 5-deaza-6-MPH_4 cofactor analogue was added in the same way as described above to make up the final concentration of 10 excess equivalents with respect to iron content. All other manipulations were the same as those above except that 10 mM L-Phe was present in all solutions. CD spectra were analyzed for eight samples without and three samples with glycerol-d_3. Four samples were prepared for VTVH MCD analysis.

Verification of the assignments of PAH^T and PAH^R states is based on methods previously described.[53] PAH activity measurements performed on the MCD samples after spectroscopic analysis showed high retention of the initial enzymatic specific activity (≥85%), indicating little sample degradation during the time course of the experimental measurements.

Instrumentation. Near-IR CD spectra (278 K, 600−2000 nm) were obtained by using a Jasco 200D spectropolarimeter with a liquid N_2-cooled InSb detector. The sample temperature was maintained by a recirculating water bath attached to the cell holder. Data acquisition was achieved by using routines written within the software package LabVIEW (National Instruments). Contributions to the CD intensity due to buffer and cell backgrounds were subtracted from the protein CD spectra. Low-temperature near-IR MCD spectra (1.6−50 K, 600−2000 nm) were obtained with the Jasco spectropolarimeter and an Oxford Instruments SM4000-7 T superconducting magnet/cryostat. Depolarization (<10%) of all frozen samples was monitored by measuring the differential CD intensity of a nickel (+)-tartrate solution placed before and after the sample compartment.[58] MCD spectra were corrected for zero-field baseline effects induced by variability in glass quality by subtracting off the corresponding 0 T scan at each temperature. Alternatively, the directionality of the applied magnetic field can be reversed by interchanging the magnet leads; this produces a "−7 T" spectrum. The subtracted average of the +7 T and −7 T scans, [7 − (−7)]/2 T, will be identical to the baseline-corrected 7 − 0 T spectrum. This protocol was employed in several cases to eliminate problems associated with glass-induced baseline shifts and to increase the signal-to-noise ratios.

(55) Stark, E.; Breitmaier, E. *Tetrahedron* **1973**, *29*, 2209−2217.
(56) Breitmaier, E.; Gassenmann, S. *Chem. Ber.* **1971**, *104*, 665−667.
(57) Moad, G.; Luthy, C. L.; Benkovic, P. A.; Benkovic, S. J. *J. Am. Chem. Soc.* **1979**, *101*, 6068−6076.
(58) Browett, W. R.; Fucaloro, A. F.; Morgan, T. V.; Stephens, P. J. *J. Am. Chem. Soc.* **1983**, *105*, 1868−1872.

Fitting Procedures. Spectra were fit to Gaussian band shapes by using a modified Levenberg−Marquardt constrained nonlinear least-squares fitting routine. Saturation magnetization data were normalized to the maximum observed intensity and fit according to published procedures to extract ground-state parameters.[45,46] Application of both the negative and positive ZFS models to the VTVH MCD data was used to determine the best fit.

Results and Analysis

A. PAH^T[5-deaza-6-MPH$_4$]. The 278 K CD spectrum of PAH^T[5-deaza-6-MPH$_4$] is shown in Figure 2A (solid line). The Gaussian resolution of the data (dashed line) indicates that two bands are present at 8900 and 10 800 cm^{-1}. This spectrum is identical with that of PAH^T[ ],[53] and the addition of glycerol-d_3 does not perturb the spectrum (data not shown). The low-temperature MCD spectrum at 5 K and 7 T of PAH^T[5-deaza-6-MPH$_4$] is shown in Figure 2B (solid line) overlaid with the corresponding spectrum of PAH^T[ ] (dashed line). The spectra are qualitatively very similar, with only a modest discrepancy in the calculated extinction coefficients. These typically vary slightly as a result of errors in concentration and path length measurements. The Gaussian resolution of the baseline-corrected PAH^T[5-deaza-6-MPH$_4$] MCD spectrum is presented in Figure 2C (dashed line) and reveals two bands at 8500 and 10 100 cm^{-1}. These transition energies centered around 10 000 cm^{-1} and split by ∼2000 cm^{-1} are consistent with a distorted octahedral ferrous active site.[45] Comparison of the CD and MCD data indicates that there is a small temperature effect on the iron site that causes the bands to be shifted to lower energy in the MCD spectrum. The similarity of the CD and MCD d → d band positions (summarized in Table 1) to those previously identified for PAH^T[ ] suggests that there is little change to the six-coordinate resting T-state ferrous center of PAH upon addition of the pterin cofactor analogue.

The temperature dependence of the PAH^T[5-deaza-6-MPH$_4$] MCD spectrum is presented in Figure 2D; the inverse relationship between MCD intensity and temperature is characteristic of *C*-term behavior arising from a degenerate electronic ground state.[45] VTVH MCD spectroscopy is an effective probe of the ground-state spin Hamiltonian parameters and d$_\pi$-orbital splittings for such high-spin ferrous non-Kramers centers.[45,46] The MCD intensity was monitored at 8805 cm^{-1} for a series of fields and temperatures. The normalized data are shown in Figure 2E plotted as a function of $\beta H/2kT$ (where β is the Bohr magneton and k is Boltzmann's constant) and in Figure 2F as a function of $1/kT$ to separate the effects of field and temperature. The nested saturation magnetization isotherms (Figure 2E) are well described by a negative ZFS non-Kramers doublet model in which the decreasing spacing between curves of equal field increments in the low-temperature region of the $1/kT$ plot (Figure 2F) is attributed to rhombic splitting of the non-Kramers doublet.[45] The data were fit by using the complete non-Kramers intensity expression given as eq 1 in ref 46. This equation includes the Zeeman interaction with low-lying excited states as $B_{i/m}$ (the B-term). The best fit to the data yields the parameters of $\delta = 2.9 \pm 0.3$ cm^{-1} and $g_{||} = 9.2 \pm 0.2$, with a small off-axis contribution ($M_z/M_{xy} = -0.06$) and a moderate linear B-term. The lower-energy component of the $M_S = \pm 1$ excited state is observed at an energy of ∼30 cm^{-1} above the ground state. On the basis of these spin Hamiltonian parameters and correlation diagrams produced from the full $^5T_{2g}$ Hamiltonian solution, which encompasses spin−orbit effects,[45] there are two possible solution sets obtained for the ligand field ground-state splitting parameters: $\Delta \approx -750$ cm^{-1} with $|V/2\Delta| \approx 0.22$ or $\Delta \approx -300$ cm^{-1} with $|V/2\Delta| \approx 0.13$. The small value of δ is unusual for a six-coordinate site; it can either be associated with π-back-bonding with a π-acceptor ligand[46,51,52] or a site that is not close to the rhombic limit ($|V/2\Delta| \approx 0.33$, which is usually appropriate for six-coordinate non-heme ferrous sites). As there is no π-acceptor ligand proposed at the active

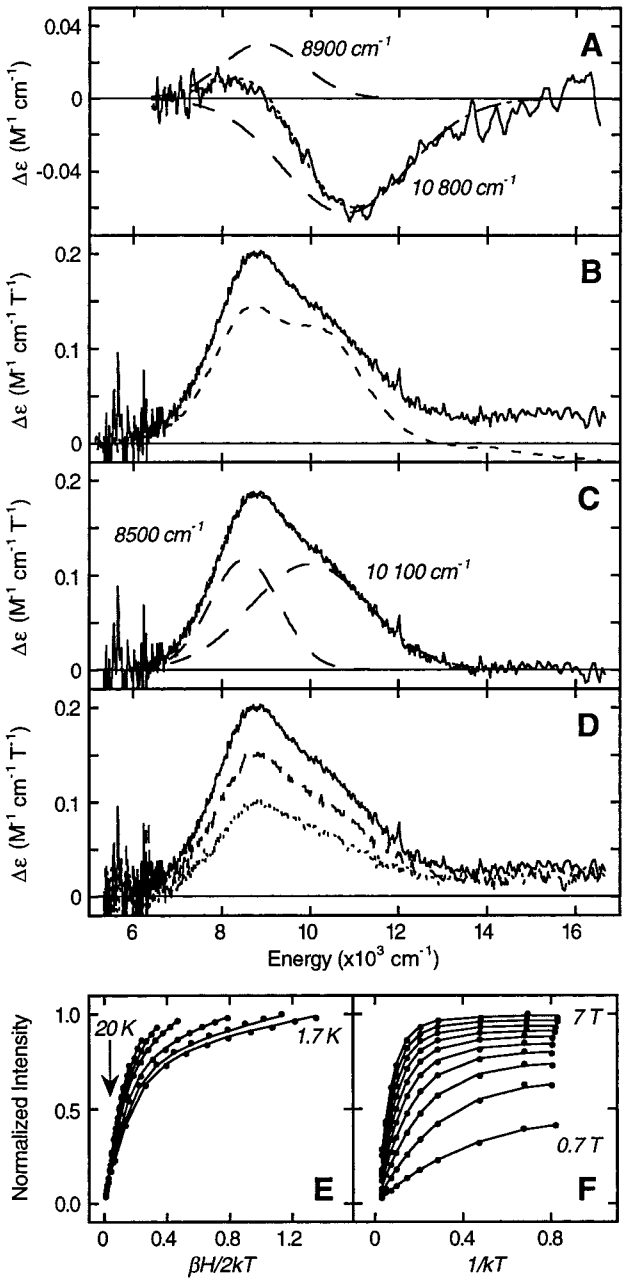

Figure 2. (A) CD spectrum at 278 K of PAH^T[5-deaza-6-MPH$_4$] (—), and the Gaussian fit (- - -) and components (— —) of the data. (B) MCD spectra at 5 K and 7 T of PAH^T[5-deaza-6-MPH$_4$] (—) and of PAH^T[ ] (- - -). (C) Gaussian fit (- - -) and components (— —) of the baseline-corrected PAH^T[5-deaza-6-MPH$_4$] MCD spectrum (—). (D) Temperature dependence of the 7 T MCD spectra of PAH^T[5-deaza-6-MPH$_4$] at 5.0 (—), 15 (— —), and 30 K (- - -). (E) VTVH saturation magnetization behavior recorded at 8805 cm^{-1} for PAH^T[5-deaza-6-MPH$_4$]. The normalized data (●) are plotted vs $\beta H/2kT$ for a series of fixed temperatures (1.7, 2.1, 3.0, 5.0, 7.0, 10, 15, and 20 K; 30 and 50 K omitted for clarity). The best fit (—) to the data was generated by the parameters described in Table 2. Errors in the data points are approximately the size of the symbol used and have been omitted for clarity. (F) The VTVH MCD data (●) and fit (—) replotted from part (E) as a function of $1/kT$ for a series of fixed fields (0.7, 1.4, 2.1, 2.8, 3.5, 4.2, 4.9, 5.6, 6.3, and 7.0 T).

Table 1. MCD Ligand Field Transition Energies

sample	glycerol	method	band 1[a,b]	band 2[a,b]	$10Dq$[a]	Δ^5E_g[a]
PAH^T[ ][c]	−/+	CD	8870	10 820	9850	1950
	+	MCD	8500	10 300	9400	1600
PAH^T[5-deaza-6-MPH_4]	−/+	CD	8900	10 800	9850	1900
	+	MCD	8500	10 100	9300	1600
PAH^{R-NEM}[ ][c]	+	MCD	8580	10 250	9420	1670
PAH^{R-NEM}[5-deaza-6-MPH_4]	+	MCD	8630	10 170	9400	1540
PAH^R[L-Phe][c]	−/+	CD	9450	11 450	10 450	2000
	+	MCD	9250	10 700	9980	1450
PAH^R[L-Phe, 5-deaza-6-MPH_4]	−	CD	<6500	11 300	<8900	>4800
	+	CD	<6500	9630	<8070	>3130
	+	MCD	≤4740	9280	≤7010	≥4540

[a] Values in cm^{-1}. [b] Error in Gaussian-resolved energies is typically ± 100 cm^{-1}. [c] Values from ref 53.

Table 2. Ground-State Spin Hamiltonian and Ligand Field Parameters

sample	δ[a]	$g_{\|\|}$	M_z/M_{xy}[b]	C-term[c]	E_s[a]	D[a]	$\|E\|$[a]	Δ[a,d]	$\|V\|$[a]	$\|V/2\Delta\|$
PAH^T[ ][e]	2.9	8.9	−0.2	1.4	28	−		−250	70	0.14
								−900	500	0.28
PAH^T[5-deaza-6MPH_4]	2.9	9.2	−0.06	1.9	26	−		−300	80	0.13
								−750	330	0.22
PAH^R[L-Phe][e]	3.7	9.5	0.08	2.4	26	−		−500	180	0.18
PAH^R[L-Phe, 5-deaza-6MPH_4]	5.2	8.0		3.0	11	8.7	1.4	+825	315	0.19

[a] Values in cm^{-1}. [b] Determined for $g_\perp$ fixed at 1.0. [c] Reported as a percentage of the C-term intensity scaling factor A_{satlim} (see ref 45). [d] $\Delta^5T_{2g} = \Delta + |V|/2$. [e] Improved methods of VTVH fitting have been developed since the initial characterization of these samples (ref 53) and differences from the previously reported parameter values are obtained and reported here (also see Supporting Information).

site of PAH,[41] the small value of δ is indicative of a less rhombic site consistent with the value of $|V/2\Delta| \approx 0.13$ with $\Delta \approx -300$ cm^{-1}. These values of the spin Hamiltonian and ligand field parameters are summarized in Table 2 and are compared with those for PAH^T[ ]. The similar saturation magnetization behavior of PAH^T[5-deaza-6-MPH_4] and PAH^T[ ] therefore confirms that pterin binding to PAH^T does not affect the geometric or electronic structure of the first coordination sphere for the ferrous active site of PAH.

B. PAH^{R-NEM}[5-deaza-6-MPH_4]. The MCD spectrum of PAH^{R-NEM}[5-deaza-6-MPH_4] taken at 5 K and 7 T is shown in Figure 3A (solid line) compared to that of PAH^{R-NEM}[ ] (dashed line). As with the T-state samples, the spectra are qualitatively very similar. Gaussian resolution of the PAH^{R-NEM}[5-deaza-6-MPH_4] MCD spectrum requires two bands at 8630 and 10 170 cm^{-1}, displayed in Figure 3B and summarized in Table 1. These maxima are nearly identical with those obtained for the NEM-activated enzyme in the absence of cofactor,[53] indicating that pterin binding does not perturb the geometry of the six-coordinate ferrous activate site of PAH^{R-NEM}. Typical C-term temperature dependence of the PAH^{R-NEM}[5-deaza-6-MPH_4] spectrum is shown in Figure 3C. As nonallosteric activation alone has been shown to have little effect on the geometric structure of the first coordination sphere of PAH,[53] and similarly the presence of the 5-deaza-6-MPH_4 pterin analogue does not perturb the site, no further spectroscopic analysis was applied.

C. PAH^R[L-Phe, 5-deaza-6-MPH_4]. The 278 K CD spectrum of PAH^R[L-Phe, 5-deaza-6-MPH_4] is shown in Figure 4A (solid line) overlaid with the spectrum of PAH^T[5-deaza-6-MPH_4] (dashed line). It is very different from the CD spectra of the resting, pterin-bound, or substrate-bound species in that the positive feature at ~8900 cm^{-1} (PAH^T[ ] and PAH^T[5-deaza-6-MPH_4]) or 9450 cm^{-1} (PAH^R[L-Phe]) is no longer present. The Gaussian resolution of the data (Figure 4B) indicates that one narrow, negative feature is present at 11 300 cm^{-1}. A single d → d transition at >10 000 cm^{-1} is indicative of a five-coordinate square-pyrimidal ferrous site; a second band should be present at ~5000 cm^{-1}.[45,46] This is not observed in CD due to protein concentration limits and the low signal-to-noise ratio in this region of the spectrum. Addition of glycerol-d_3 to the sample eliminates the 11 300 cm^{-1} CD band and a single positive feature at 9630 cm^{-1} is now observed (dashed line in Figure 4C).

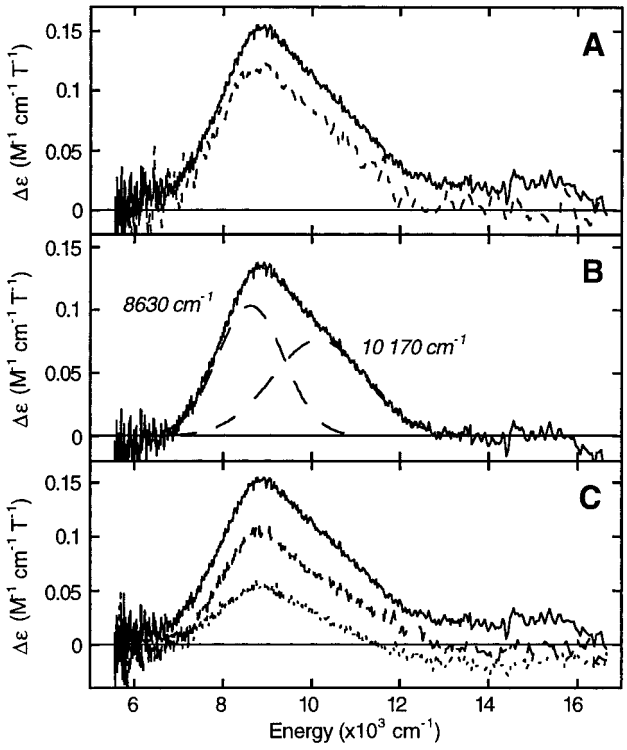

Figure 3. (A) MCD spectra at 5 K and 7 T of PAH^{R-NEM}[5-deaza-6-MPH_4] (—) and of PAH^{R-NEM}[ ] (- - -). (B) Gaussian fit (- - -) and components (— —) of the baseline-corrected PAH^{R-NEM}[5-deaza-6-MPH_4] MCD spectrum (—). (C) Temperature dependence of the 7 T MCD spectra of PAH^{R-NEM}[5-deaza-6-MPH_4] at 5.0 (—), 15 (— —), and 35 K (- - -).

The MCD spectrum of PAH^R[L-Phe, 5-deaza-6-MPH_4] is shown in Figure 5A as the subtracted average of the 7 T and −7 T data at 5 K (solid line) overlaid with the 5 K, 7 T spectrum

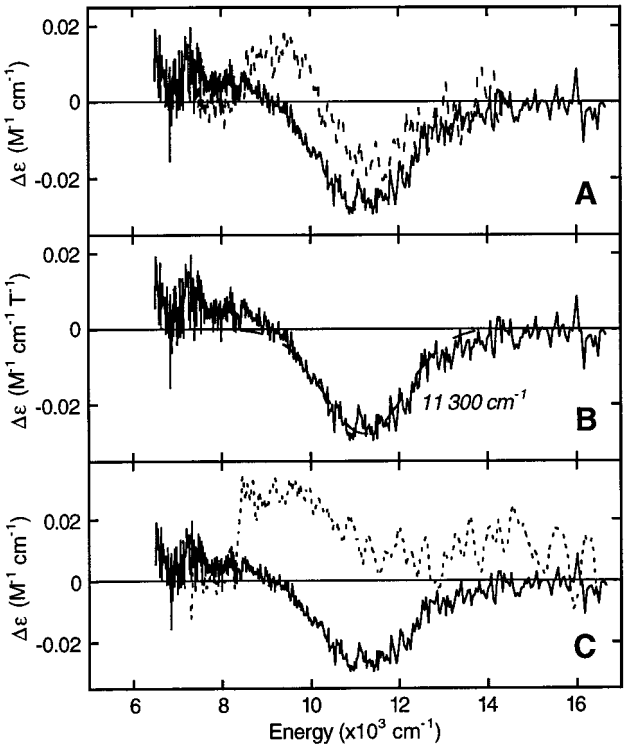

Figure 4. (A) CD spectrum at 278 K of PAH^{R}[L-Phe, 5-deaza-6MPH$_4$] (—) and of PAH^{R}[L-Phe] (- - -). (B) Gaussian fit (- - -) and components (— —) of the PAH^{R}[5-deaza-6-MPH$_4$] CD spectrum (—). (C) CD spectrum of PAH^{R}[L-Phe, 5-deaza-6MPH$_4$] at 278 K without glycerol-d_3 (—) and with glycerol-d_3 (- - -).

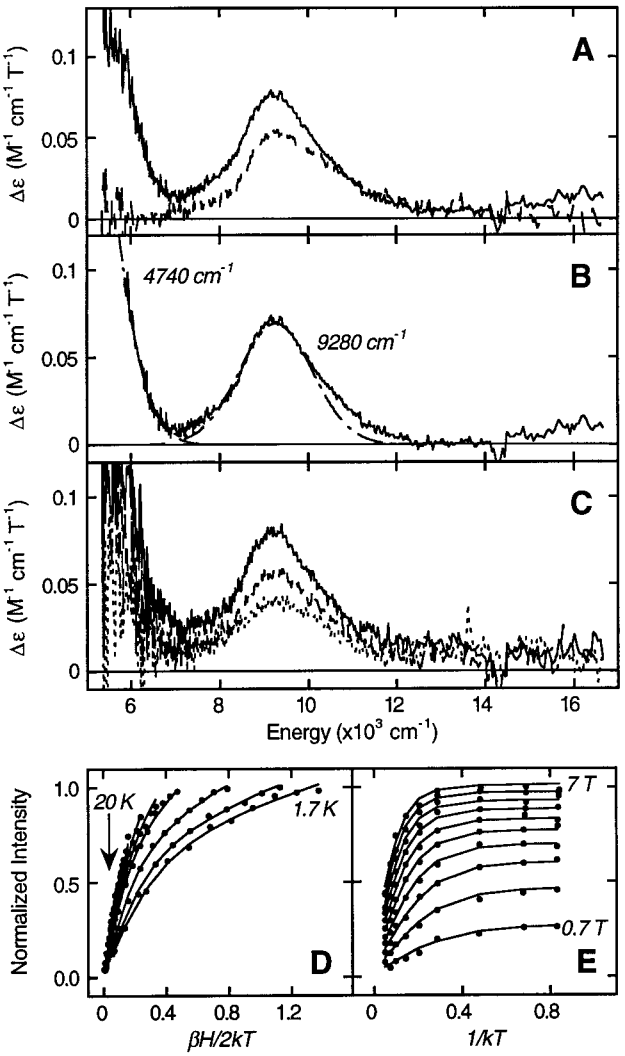

Figure 5. (A) MCD spectra at 5 K and [7 − (−7)]/2 T of PAH^{R}[L-Phe, 5-deaza-6-MPH$_4$] (—) and at 5 K and 7 T of PAH^{R}[L-Phe] (- - -). (B) Gaussian fit (- - -) and components (— —) of the baseline-corrected PAH^{R}[L-Phe, 5-deaza-6MPH$_4$] spectrum (—). (C) Temperature dependence of the −7 T MCD spectra of PAH^{R}[L-Phe, 5-deaza-6-MPH$_4$] at 5.0 (—), 15 (- - -), and 30 K (— —). (D) VTVH saturation magnetization behavior recorded at 6055 cm^{-1}. The normalized data (●) are plotted vs $\beta H/2kT$ for a series of fixed temperatures (1.7, 2.1, 3.0, 5.0, 7.0, 10, 15, and 20 K; 30 and 50 K omitted for clarity). The best fit (—) to the data was generated by the parameters described in Table 2. Errors in the data points are approximately twice the symbol size used and have been omitted for clarity. (E) The VTVH MCD data (●) and fit (—) replotted from part (D) as a function of $1/kT$ for a series of fixed fields (0.7, 1.4, 2.1, 2.8, 3.5, 4.2, 4.9, 5.6, 6.3, and 7.0 T).

of PAH^{R}[L-Phe] (dashed line). There is relatively little difference in the positions of the maxima near 9300 cm^{-1}; however, there is a considerable intensity increase at low energy for the new cofactor-bound species. The Gaussian resolution of the PAH^{R}[L-Phe, 5-deaza-6-MPH$_4$] spectrum is shown in Figure 5B and requires one band at 9280 cm^{-1} and a second band below ∼4740 cm^{-1}. The position of the higher-energy band indicates that there is little change in the active site due to temperature. The presence of two bands at ∼10 000 and ∼5000 cm^{-1} indicates that the combination of allosteric activation and the presence of both substrate and cofactor leads to a five-coordinate site. Spectra of samples in which the order of addition of 5-deaza-6-MPH$_4$ and L-Phe was varied indicate that the formation of this five-coordinate site is not dependent on the order of addition of substrate and cofactor analogue. Similar spectral features have also been observed for the NEM-activated species, PAH^{R-NEM}[L-Phe, 5-deaza-6-MPH$_4$].[59] Numerous attempts to trap the PAH^{T}[L-Phe, 5-deaza-6-MPH$_4$] species led to fully activated enzyme. Additionally, experiments with sucrose as an alternative glassing agent led to another perturbed five-coordinate site (different from that obtained with glycerol-d_3) and poor glasses that were unsuitable for MCD experiments.

The temperature dependence of the PAH^{R}[L-Phe, 5-deaza-6-MPH$_4$] spectrum is presented in Figure 5C and displays typical *C*-term behavior of decreasing intensity with increasing temperature. VTVH MCD data were collected on both d → d bands for a series of fixed fields and temperatures; the data collected at 6055 cm^{-1} are plotted in Figure 5D vs $\beta H/2kT$ and in Figure 5E vs $1/kT$ to separate the effects of field and temperature. The data were fit initially by using a negative ZFS model which assumes the nesting behavior results from rhombic splitting of the $M_S = \pm 2$ non-Kramers doublet ground state.[45] This fit resulted in a large value of δ and the presence of a low-lying singlet excited state. Together these results are suggestive of a positive ZFS ferrous system for which the $M_S = 0$ level is lowest in energy and has pseudo non-Kramers doublet behavior with one component of the $M_S = \pm 1$ excited state; the second $M_S = \pm 1$ component is treated as an MCD-silent singlet.[47] Applying this three-level model with $g_{||}$ fixed at 8.0, the best fit to the data yields a pseudo-doublet splitting of 5.2 ± 0.3 cm^{-1}, a moderate *B*-term contribution, and a singlet excited-state energy of $E_S \approx 11$ cm^{-1}. The experimentally determined energies of this spin manifold (at 0, 5.2, and 13.6 cm^{-1}) can be used to solve for the axial and rhombic ZFS spin Hamiltonian and ligand field models[45] to obtain $D = 8.7 \pm 0.2$ cm^{-1}, $|E| = 1.4 \pm 0.2$

(59) Kemsley, J. N.; Mitic, N.; Caradonna, J. P.; Solomon, E. I. Unpublished data.

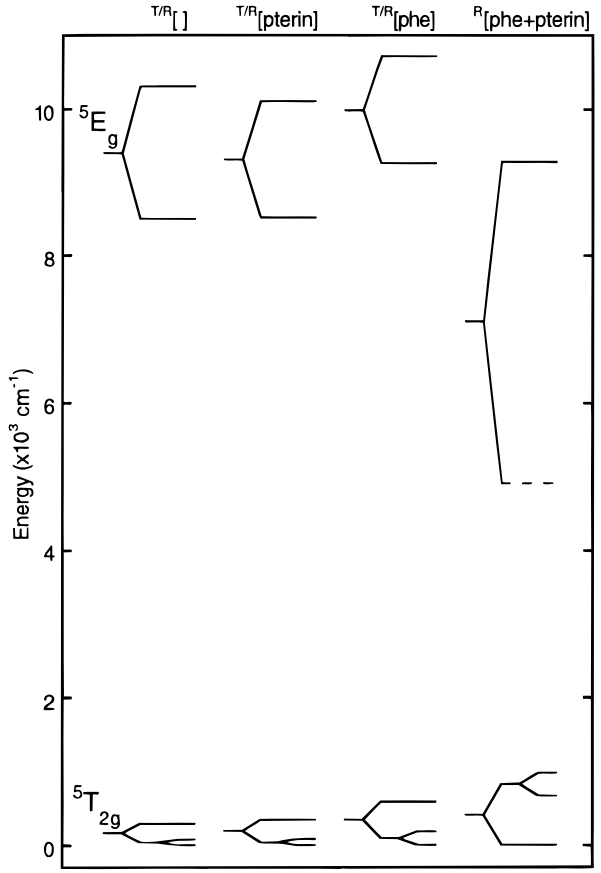

Figure 6. Experimentally determined d-orbital energy levels for $PAH^{T/R}$[ ], $PAH^{T/R}$[5-deaza-6-MPH_4], $PAH^{T/R}$[L-Phe], and PAH^{R}[L-Phe, 5-deaza-6-MPH_4]. The dashed line indicates that the energy is not well determined.

cm^{-1}, $\Delta \approx +825$ cm^{-1}, and $|V/2\Delta| \approx 0.19$. These values are summarized in Table 2.

D. Summary of d-Orbital Energy Levels. From the experimental excited-state splittings and ground-state VTVH analyses, complete experimental d-orbital energy level diagrams have been constructed for PAH^{T}[5-deaza-6-MPH_4] and PAH^{R}[L-Phe, 5-deaza-6-MPH_4] and are presented in Figure 6. For PAH^{T}[5-deaza-6-MPH_4] the observed ^5E_g excited-state d_σ-orbital energies at 8500 and 10 100 cm^{-1} are consistent with distorted octahedral coordination for the ferrous center. The $^5T_{2g}$ ground-state d_π-orbitals lie at 0, 80, and 340 cm^{-1}, as observed for six-coordinate complexes of oxygen and nitrogen ligations.[46] The energies of these five d-orbitals are virtually unchanged relative to those of resting PAH^{T}[ ], suggesting that the presence of pterin cofactor does not influence the geometric or electronic structure of the ferrous site of PAH. The observed excited-state energies for PAH^{R}[L-Phe, 5-deaza-6-MPH_4] occur at $\leq$4740 and 9280 cm^{-1} and the large splitting between the d_{z^2} and $d_{x^2-y^2}$ orbitals is consistent with a distorted five-coordinate environment at the metal center. These orbitals have a relatively small splitting for five-coordinate sites, indicating a square-pyramidal geometry with a strong axial interaction.[46] The splitting of the ground-state orbitals also increases with their energies at 0, 670, and 980 cm^{-1}, which is in a range consistent with five-coordinate complexes of similar oxygen and nitrogen ligation; positive ZFS is also consistent with a strong-axial square-pyramidal structure.[46] As the d $\rightarrow$ d transitions observed in the MCD spectra of all other PAH species examined so far, including PAH^{R}[L-Phe] and PAH^{R-NEM}[5-deaza-6-MPH_4], show a small splitting of the d_σ-orbitals indicating six-coordinate geometric structures, these results indicate that the conversion to the five-coordinate PAH^{R}[L-Phe, 5-deaza-6-MPH_4] species occurs for the activated enzyme only in the presence of both substrate and cofactor. This finding may have significant relevance to the sequential mechanistic order that requires assembly of this ternary species prior to dioxygen reaction and catalysis.

Discussion

Phenylalanine hydroxylase is an important enzyme for its metabolic function and association with PKU, but there is little information regarding the catalytically competent ferrous oxidation state of the active site iron and its role in the hydroxylation mechanism. Using CD, MCD, and XAS spectroscopies we previously demonstrated that the ferrous active site of resting PAH^{T}[ ] is six-coordinate distorted octahedral with significant oxygen ligation.[53] Whereas allosteric and nonallosteric activation did not alter the geometric structure of this site, the addition of substrate to the catalytic site produced a perturbed six-coordinate structure with an increased ligand field strength. This perturbation was proposed to help orient the substrate for coupled hydroxylation. The PAH system is further complicated by its unique tetrahydropterin dependence. This includes the use of BH_4 to reduce the enzyme from Fe^{3+} to Fe^{2+} and the requirement of additional BH_4 as a cosubstrate in the catalytic reaction. We have now extended our spectroscopic approach to investigate the interaction of a cofactor analogue of BH_4 with the ferrous active site of PAH, in the absence and presence of L-Phe.

From the similarities in the excited-state ligand field transition energies in the near-IR CD and MCD spectra of PAH^{T}[ ] and PAH^{T}[5-deaza-6-MPH_4], and the ground-state orbital splittings determined from VTVH MCD analyses of these samples, the presence of the cofactor does not alter the geometric or electronic structure of the reduced, resting T-state active site. Addition of cofactor to nonallosterically activated PAH^{R-NEM}[ ] also produces similar spectral features to those observed in the absence of cofactor, indicating that the pterin does not perturb the active site geometry of this activated form of the enzyme, which is consistent with crystallographic analysis of the cofactor analogue 7,8-dihydrobiopterin bound to tyrosine hydroxylase.[60] This is in contrast to the interaction of the non-heme iron enzyme clavaminate synthase-2 (CS2) with its cofactor, α-ketoglutarate (α-KG), where α-KG displaces two ligands from the six-coordinate resting active site of CS2 to form a new six-coordinate α-KG-bound ferrous site.[52] This difference in active site interactions may be due to the relative reactivities of the cofactors: α-KG is not redox active and must be activated by the iron whereas the pterin cofactor is redox active and may not need to coordinate to participate in the catalytic reaction.

There are at least four independent methods of activating PAH and inducing the T $\rightarrow$ R conversion that is manifested in several properties of the enzyme, most notably in an increase in the rate of turnover and a change from sigmoidal to hyperbolic kinetics.[12,37] It has been proposed that the $PAH^{T} \rightarrow PAH^{R}$ reorganization acts to transform a regulatory pterin binding site into a catalytic site without altering the inner coordination sphere of the iron center.[37,38,61] The spectroscopic data reported herein on allosterically- and NEM-activated PAH offer the first direct

(60) Goodwill, K. E.; Sabatier, C.; Stevens, R. C. *Biochemistry* **1998**, *37*, 13437−13445.
(61) Shiman, R.; Gray, D. W.; Hill, M. A. *J. Biol. Chem.* **1994**, *269*, 24637−24646.

evidence that the interaction of the protein with the pterin alone does not influence the structure of the ferrous active site. Along with our previous data indicating that the ferrous site of $PAH^{T}[\ ] = PAH^{R-NEM}[\ ]$ and PAH^{T}[L-Phe] = PAH^{R}[L-Phe], this supports the idea that the T → R reorganization affects the local environment of the metal center but does not directly affect the iron site.

Addition of cofactor *and* substrate to activated PAH, however, results in a large splitting of the ligand field bands indicating a five-coordinate active site geometry. The energy of the d → d transition observed by CD is consistent with a square-pyramidal site with a weak axial interaction. This interaction becomes stronger upon addition of glycerol-d_3. The crystal structure has been solved for the catalytic domain of the ferric enzyme (≈$PAH^{R}[\ ]$, without the regulatory domain)[41] and confirms earlier site-directed mutagenesis studies that indicated His285 and His290 are active site ligands.[62] The remaining iron ligands are monodentate Glu330 and three waters.[41] It has been proposed that pterin binding is localized to residues His263 to His289,[63] while residues involved in substrate binding have not been identified. Thus both histidine ligands may be perturbed by pterin binding and may be involved in the loss of an Fe^{2+} ligand for PAH^{R}[L-Phe, 5-deaza-6-MPH_4] and the change in the axial ligand field strength. With only three endogenous ligands reported for the six-coordinate site,[41] it is likely that the endogeneous ligand perturbation associated with substrate and pterin binding results in loss of a water to generate the five-coordinate ferrous active site.

The observed sequential mechanistic order for resting PAH is L-Phe + BH_4 + O_2.[31,38,39] Addition of L-Phe is required prior to BH_4 as the presence of the natural cofactor will competitively inhibit allosteric activation. Once the enzyme is activated, the binding of L-Phe to PAH^{R} is noncompetitive with respect to BH_4 and 5-deaza-6-MPH_4, suggesting that the hydroxylation reaction proceeds through a single enzyme−substrate complex.[11,19,37] Sufficient L-Phe will conformationally perturb the active site geometry[53] and this is required in order for the addition of pterin to yield the newly observed five-coordinate structure of the PAH^{R}[L-Phe, 5-deaza-6-MPH_4] complex, as evidenced by the increased excited-state ^5E_g and ground-state $^5T_{2g}$ orbital splittings. Our results are therefore in accord with the ordered mechanism requiring formation of the ternary complex, with the first evidence of an open coordination position on the iron prior to binding and activation of dioxygen. This directly implicates the iron in the coupled hydroxylation of substrate and cofactor: the pterin could react with O_2 leading to a reactive bridged-peroxy-Fe intermediate,[23] or the metal could form an active oxygen species prior to its reaction with pterin and L-Phe.[24] Neither possibility may occur without the presence of both substrates involved in coupled hydroxylation, consistent with the generation of a highly reactive oxygen intermediate in close proximity to substrate.

In summary, CD and MCD spectroscopies have been employed to obtain the first direct information about the interactions of Fe^{2+}, L-Phe, and pterin cofactor in PAH reactivity. While addition of pterin alone to the enzyme does not perturb the six-coordinate iron active site, addition of both pterin and L-Phe results in a five-coordinate species. The opening of a coordination position prior to coupled hydroxylation implicates the direct involvement of the ferrous site in the catalytic activity of PAH. These experiments are currently being extended to probe the effects of key amino acid mutations on the formation of the five-coordinate active site and coupled hydroxylation.

Acknowledgment. This work was supported by grants from the National Institutes of Health (GM40392, E.I.S.), the American Chemical Society (25963AC, J.P.C.), and the Camille and Henry Dreyfus and Alfred P. Sloan Foundations (J.P.C.). J.N.K. would like to thank the National Institutes of Health for a biotechnology training grant (GM08412). The computing facilities of the Department of Chemistry at Stanford University are supported in part by a grant from the National Science Foundation (CHE-9408185).

Supporting Information Available: VTVH MCD spectroscopic analysis of $PAH^{T}[\ ]$ and PAH^{R}[L-Phe] (PDF). This material is available free of charge via the Internet at http://pubs.acs.org.

JA9833063

(62) Gibbs, B. S.; Wojchowski, D.; Benkovic, S. J. *J. Biol. Chem.* **1993**, *268*, 8046−8052.

(63) Jennings, I. G.; Kemp, B. E.; Cotton, R. G. H. *Proc. Natl. Acad. Sci. U.S.A.* **1991**, *88*, 5734−5738.